

Nitrilotriacetic acid functionalization on Fe₃O₄ nanoparticle via amino and carboxylic functionalization

Jin Soon Han^{a,**}, MiRae Youm^{a,**}, Hyun-Hee Choi^b, Yeon-Gil Jung^b, Sung-Churl Choi^a and Gye Seok An^{a,*}

^aHanyang university 04763 Division of Materials Science and Engineering, Hanyang University, 222 Wangsimni-ro, Seongdong-gu, Republic of Korea

^bSchool of Materials Science and Engineering, Changwon National University, 20 Changwondaehak-ro, Changwon, Gyeongnam 51140, Republic of Korea

Since chelating chemical had focused for enhancing bio-susceptibility and ability for the binding with biomaterials, in this study, Nitrilotriacetic acid (NTA) was utilized for the developing chelate ligand attached superparamagnetic nanoparticle. In order to conjugate NTA, carboxylic group was needed on the surface of substrate particle for building peptide bond with amine group which was branched from the NTA structure. Therefore Fe₃O₄ nanoparticle was functionalized with various of amine precursor (Polyethyleneimine (PEI), (3-Aminopropyl)triethoxysilane (APTES)), and carboxyl precursor (Polyacrylic acid (PAA)) before the conjugation of NTA. Then NTA conjugation behavior was estimated which is varied with the type of amine precursor which affects to the surface properties.

Keywords: Magnetic nanoparticle, Chelate ligand, Nitrilotriacetic acid, Functionalization.

Introduction

Chelate-based sensors play an important role in environmental and biological fields as metal and chemical detectors, humidity sensors, and biosensors, among others [1-5]. Metal ions act as stimulators by attaching solely to the chelate ligand on the surface of the sensing particle; however, the sensing particles can be stimulated by the secondly attached chemical on the particular pair of chelate and metal ion. These mechanisms were usually determined by the types of chelates, which were represented by nitrilotriacetic acid (NTA), ethylenediamine diacetate (EDDA), and ethylenediaminetetraacetic acid (EDTA) with different functional groups and affinities for other materials [6]. Owing to these mechanisms, chelates have been applied for sensing metal ions, chemical reagents, and biomaterials. Especially in the case of biosensors, they have been utilized for sensing protein or DNA, which is directly connected to protein and genetic engineering [5, 9, 10].

To reinforcing sensing and recollecting, the introduction of magnetic properties was assumed as an effective way for mass controlling particles by inducing a magnetic field. Fe₃O₄, in particular, has paramagnetic properties that ensure reversible mobility in a sensor particle. Therefore, nanoparticles having higher efficiency than

the first attached substrate have been utilized [10-14]. The surface plasmon resonance (SPR) bio-sensor chip was based on the high refractive index of Fe₃O₄, which was directly connected to the efficiency [15, 16]. In the case of NTA, as an enzyme-free biosensor, the efficiency of the sensor and controllability of nanoparticles have been the areas of focus [14, 17].

However, nanoparticles were reported to have unexpected toxicity that could cause DNA damage. There are many factors that determine the toxicity of nanoparticles, including its concentration, particle size, existence of coating layer, and total surface area [18].

To further functionalize Fe₃O₄, various types of materials were applied on its surface, such as noble metals, carbon materials, and other chemical reagents [10-13]. For example, Fe₃O₄-Au composite particle coated with horseradish peroxidase was utilized with graphene sheets-Nafion film for detecting hydrogen peroxide based on its high surface activity [11]. Carbon-coated Fe₃O₄ with TiO₂ layer was used as a photoelectrochemical biosensor for uric acid [12]. In the case of NTA, NTA had been built on intermediate polyacrylamide via the polymerization process for separating his-tagged protein. Since γ -methacryloxypropyl trimethoxysilane was polymerized to prepare the substrate layer of NTA, the magnetic property of NTA attached Fe₃O₄ nanoparticle was reinforced; however, this requires certain conditions, including prolonged reflux and noble gas injection for protection [14].

In order to utilize this NTA conjugating method into mass production, building these conditions with large

*Corresponding author:

Tel : +8222200505

Fax: +8222916767

E-mail: faustmaro@hanyang.ac.kr

**These authors contributed equally to this work.

scale were not preferred. And the magnetic properties about Fe_3O_4 nanoparticle had been decreased after the NTA conjugation with reflux condition. With these aspect, utilizing the NTA attached Fe_3O_4 nanoparticle into genetic or protein technology had been carried out only in a small scale, and another method had to be established in order to get over this situation.

In this study, we methodologically reviewed the effects of intermediate functionalization on the NTA attachment process on the surface of Fe_3O_4 and the properties of NTA-attached Fe_3O_4 nanoparticles. In the first method, (3-aminopropyl)triethoxysilane (APTES) and polyethylenimine (PEI) were utilized to attach the amine group on the Fe_3O_4 nanoparticle. Then, NTA was conjugated with the cross-linker before the amino-functionalized Fe_3O_4 nanoparticle and NTA. The second method involved direct conjugation via carboxylic functionalization with polyacrylic acid (PAA), which did not require a cross-linker between the particle and NTA. By comparing these samples, a more adequate method for fabricating NTA attached Fe_3O_4 nanoparticle was established.

Experimental Procedure

Materials

The Fe_3O_4 nanoparticles were prepared as starting materials following a previously reported polyol-based method. [19, 20] APTES (Sigma Aldrich, USA) and PEI (M_w : ~25,000, branched, Sigma Aldrich, USA) were used for amino functionalization, and PAA (M_w ~450,000, Sigma Aldrich, USA) was used for carboxylic functionalization. Then, $N\alpha, N\alpha$ -Bis(carboxymethyl)-L-lysine hydrate (ABNTA, $\text{C}_{10}\text{H}_{18}\text{N}_2\text{O}_6 \cdot x\text{H}_2\text{O}$, Sigma Aldrich, USA) was prepared as a chelate chemical. Glutaraldehyde solution (GLH; 25%, Sigma Aldrich, USA) was also prepared for the cross-linker.

Amino functionalization using APTES with the core-shell $\text{Fe}_3\text{O}_4@/\text{SiO}_2$ nanoparticle

Fe_3O_4 nanoparticles (2 g) were prepared with a mixed solvent containing 450 mL ethyl alcohol and 50 mL distilled water after the previously reported in-situ SiO_2 coating process [19, 20, 27]. The dispersed solution was set for stabilization and adjusted to basic pH. Then, 4 wt% of APTES was injected dropwise as an ethyl alcohol-based solution for the amine attached silicate precursor. After 8 h of vigorous stirring, the amino-functionalized nanoparticle was collected by the magnetic field and washed with ethyl alcohol and distilled water for several times.

Amino functionalization using PEI with Fe_3O_4 nanoparticle

The prepared Fe_3O_4 nanoparticles (2 g) were dissolved in 100 mL of distilled water and 4 wt% of PEI solution. Next, this solution was mixed for 30 min

at room temperature before heating to 80 °C. It was then reacted for 10 h with vigorous stirring and cooled down until it reached the room temperature. The reacted particle nanoparticle was collected by inducing magnetic field and stored as a solution with distilled water after washing it several times with distilled water.

Formation of NTA chelating ligand on the surface of amino-functionalized Fe_3O_4

A total of 0.1 g of both distinctly amino-functionalized Fe_3O_4 nanoparticles with APTES and PEI were prepared as a solution with 100 mL of distilled water and mechanically stirred before the reaction. Then, the glutaraldehyde solution was injected and mechanically stirred for 8 h [21]. The particles were collected via the induced magnetic field and washed with distilled water for removing the unreacted reagent and modifying their acidity to the neutral state. Then, they were re-dispersed at 100 mL of distilled water and mixed with the ABNTA solution. Reaction occurred under the vigorous stirring condition at room temperature for 24 h. Finally, the chelating ligand-attached Fe_3O_4 nanoparticles were collected via magnets. It was then washed and stored with distilled water.

Chelate functionalization of Fe_3O_4 nanoparticle via carboxylic functionalization with PAA

A dispersed solution (300 mL) containing 10 g Fe_3O_4 nanoparticles was prepared after washing several times with distilled water. Then, PAA was prepared as a 100 mL solution with 4 wt% of concentration. These solutions were mixed in a round bottom flask and heated to 75 °C for 4 h. The mixed solution was mechanically stirred at 300 rpm until the solution cooled down to room temperature. Next, 0.25 g of PAA-attached Fe_3O_4 was re-dispersed in 100 mL distilled water and mixed with 100 mL ABNTA to obtain a concentration of 0.1 wt%. These solutions were reacted for 8 h via mechanical stirring. Then, the reacted Fe_3O_4 nanoparticle was washed and stored in distilled water.

Characterization

The surface functional group of as-synthesized Fe_3O_4 , amino-functionalized Fe_3O_4 , and NTA-attached Fe_3O_4 was analyzed via Fourier-transform infrared spectroscopy (FTIR, IRAffinity-1S, Shimadzu, Japan) at 500 ~ 4,000 cm^{-1} . The FTIR spectra was used to judge the success of functionalization of Fe_3O_4 with the existing peaks of amine or carboxyl group of APTES, PEI, and NTA and the differences in micro structure between different amine reagents. Microscopic analysis was also conducted using a transmittance electron microscope (HRTEM, Tecnai G2 F30 S-Twin, FEI, Netherlands) for the visual identification of the coating layer on Fe_3O_4 particles. Then, using the Zeta potential (Zetasizer, Malvern, USA), the changes on the surface

charges of Fe_3O_4 particles were observed after amino functionalization and NTA attaching. Finally, the magnetic properties of the as-synthesized and NTA-attached Fe_3O_4 particles were identified using a vibrating sample magnetometer (VSM, Lake shore 7400, USA).

Results and Discussion

Morphological changes of Fe_3O_4 and intermediate functionalized Fe_3O_4

A transmittance electron microscopy (TEM) analysis was performed to examine the surface and microstructure of the as-synthesized Fe_3O_4 nanoparticles, amino-functionalized Fe_3O_4 with APTES and PEI, and carboxyl-functionalized Fe_3O_4 with PAA (Fig. 1). The as-synthesized Fe_3O_4 nanoparticles were observed about 300 nm in size. In the case of APTES-modified particles, the observed particle size and the morphology were almost identical to those of the as-synthesized

particle. However, the Fe_3O_4 particles functionalized with PEI were found to be semi-spherical in shape, with a size of approximately 300 nm. A coated layer with a thickness of 3 ~ 4 nm was formed on the surface of the PEI-treated Fe_3O_4 particles. In contrast, to be functionalized into carboxylic acid, the PAA-treated Fe_3O_4 nanoparticles had a smooth and opaque layer on their surface, with a thickness of 5–6 nm. The core size of PAA-treated Fe_3O_4 was approximately 320 nm, which was slightly greater than the as-synthesized Fe_3O_4 , and it had an almost perfectly spherical shape, in comparison with the PEI-treated Fe_3O_4 particles.

Functional group on the Fe_3O_4 and intermediate functionalized Fe_3O_4

The FT-IR spectra of as-synthesized Fe_3O_4 , amino-functionalized Fe_3O_4 with APTES and PEI, and carboxyl-functionalized Fe_3O_4 with PAA are illustrated in Fig. 2. The Fe–O peak was observed at around 600

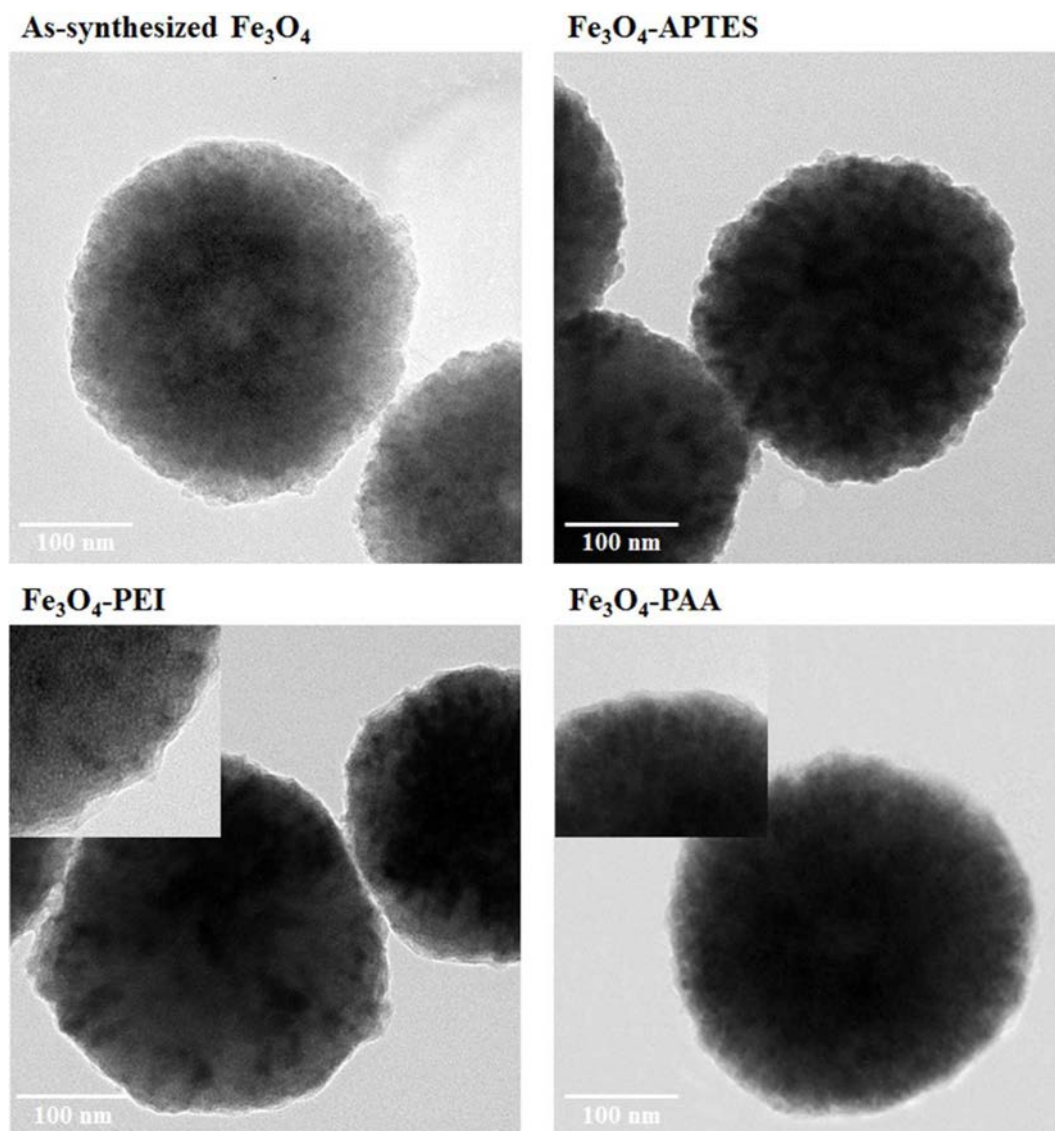


Fig. 1. TEM images of as-synthesized Fe_3O_4 and intermediate functionalized Fe_3O_4 particles.

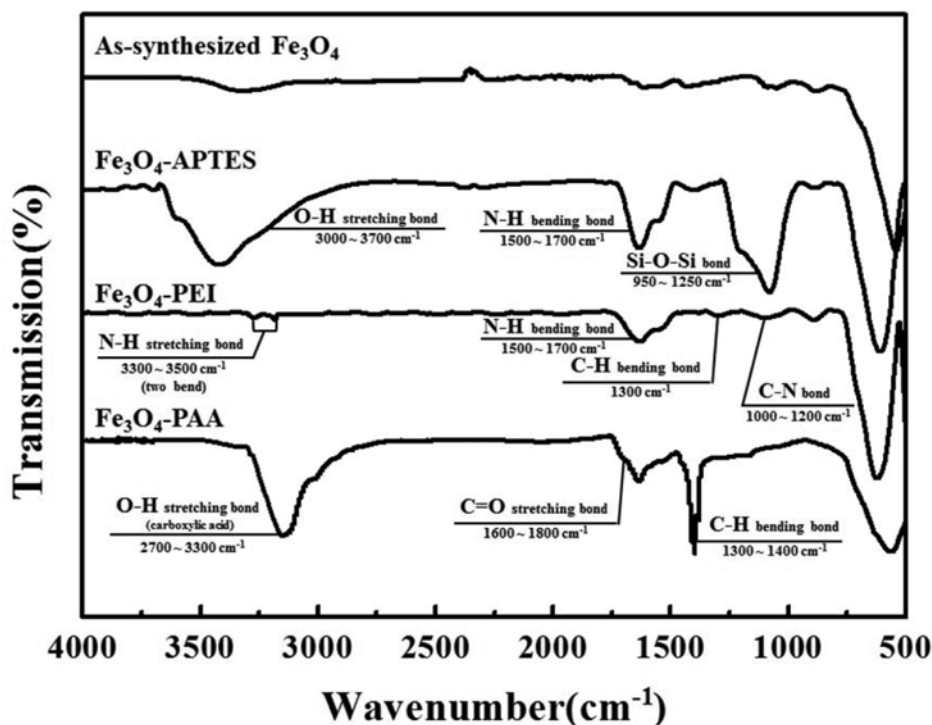


Fig. 2. FT-IR spectra of as-synthesized Fe_3O_4 and intermediate functionalized Fe_3O_4 particles.

cm^{-1} for each particle [22]. After surface modification, a distinctive amine peak was observed at $1,500 \sim 1,700 \text{ cm}^{-1}$ owing to the bending of the N-H bending bond. Because the condensation of SiO_2 was accompanied by the functionalization of APTES, an O-H stretching peak and Si-O-Si peak were observed at around $3,000$ and $950 \sim 1,250 \text{ cm}^{-1}$, respectively. In the case of another amino functionalization with PEI, the polymeric carbon chains were stuck on the surface of the particle; thus, the C-H bending peaks were observed at $1,300 \text{ cm}^{-1}$. Additionally, in the spectrum of PEI used particle, C-N bending and N-H stretching bonds were observed at $1,000 \sim 1,200$ and $3,300 \sim 3,500 \text{ cm}^{-1}$, respectively, and these ranges were where the intensive peaks from O-H stretching bond and Si-O-Si bond were found in the spectrum of the APTES used particle [22, 23, 25]. Although some differences were observed, it was confirmed that both surface-treated particles were successfully functionalized with the amine group. In contrast, in the case of PAA treatment, the C-H bending bond derived from the polymeric carbon chain was observed at $1,300 \sim 1,400 \text{ cm}^{-1}$, which was similar to the PEI-treated particles. Significant carboxylic bonds were also found at $1,600 \sim 1,800$ and $3,000 \text{ cm}^{-1}$ for the C=O and O-H stretching bonds, respectively. The O-H stretching bonds were observed at $2,700 \sim 3,300 \text{ cm}^{-1}$, which was slightly lower than the range for the APTES-treated particles ($3,000 \sim 3,700 \text{ cm}^{-1}$) [25]. Considering the difference in the O-H stretching bond, we determined that the carboxyl group was successfully attached on the surface of Fe_3O_4 and that most of the

O-H bonds originated from the carboxylic acid instead of the hydroxyl group.

Discussion about intermediate functionalization process of Fe_3O_4

As mentioned above, differences were observed in the amino-functionalized particles with APTES and PEI, from the aforementioned analysis. The functionalization mechanism with APTES is based on hydrolysis and condensation, similar to the Stöber method [23]. During APTES treatment, the existing SiO_2 layer was etched with an ammonia solution, and the unreacted hydroxyl groups were exposed via a hydrolysis reaction. These hydroxyl groups were used for the condensation site with APTES, and this functional group was observed in the FT-IR spectrum of Fe_3O_4 with APTES, at $3,000 \sim 3,700 \text{ cm}^{-1}$. However, as evident in the functionalized Fe_3O_4 with PEI and PAA, the functionalization process did not include an intermediate layer; thus, these precursors were directly attached to the surface of the Fe_3O_4 nanoparticles. However, owing to the molecular structure of APTES, Si-O-Si bond could not be formed continuously; thus, the coated layer was not observed on the surface of APTES-treated particles. In the case of PEI- and PAA-treated particles, directly bound carbon chains created an opaque layer on the surface of the Fe_3O_4 nanoparticle.

Scheme about NTA conjugation and intermediate functionalization process of Fe_3O_4

Fig. 3 shows the chemical structures of Fe_3O_4

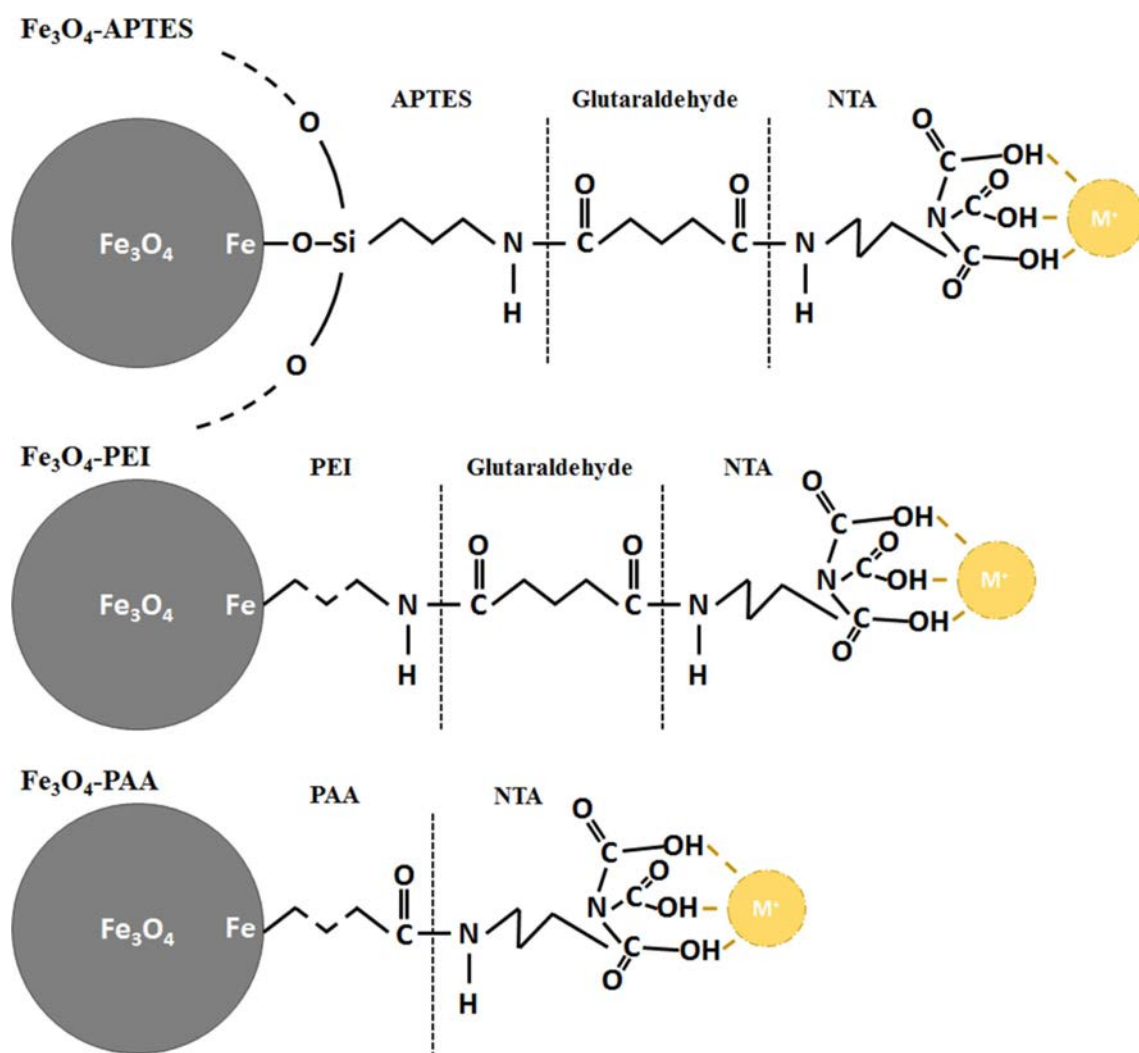


Fig. 3. Scheme of chemical structures of NTA conjugated Fe_3O_4 particles through various types of intermediate functionalization.

functionalized using various methods, along with a brief scheme of the NTA-attaching mechanism on the surface of Fe_3O_4 nanoparticles. Because a condensation reaction involving electrostatic attraction was used in the NTA-attaching mechanism, in the case of amine, the Fe_3O_4 particles were attached with glutaraldehyde before the conjugation with NTA. As evident from the FT-IR spectra, the intermediate SiO_2 layer or carbon chain exhibited the most significant difference between APTES- and PEI-treated Fe_3O_4 . This difference could derive different conjugation properties with glutaraldehyde owing to the different concentrations of activation sites, electrostatic force, and chemical affinity with glutaraldehyde. Then, glutaraldehyde formed another peptide bond with the amine group of NTA, which could attach with several metal ions, such as Ni and W. However, PAA-treated Fe_3O_4 particles contained carboxylic acid, which could form peptide bonds with the amine group. Therefore, PAA-treated Fe_3O_4 could be conjugated with NTA directly, and glutaraldehyde was not required as a cross-linker. The absence of a

cross-linker and the reversal in the pH value and surface charge were different for the APTES- and PEI-treated particles, and these could be affected after the NTA conjugation.

Morphological changes of NTA conjugated Fe_3O_4

The FT-IR spectra of NTA-attached Fe_3O_4 particles obtained via various types of intermediate functionalization are shown in Fig. 4. An emphasized peak was observed in the spectrum of the NTA-attached particles, in contrast to the APTES-attached particles. Distinctive peaks, which were observed in the FT-IR spectrum of Fe_3O_4 with APTES shown in Fig. 2, were also observed at 600 cm^{-1} (Fe-O) and $1,300\text{ cm}^{-1}$ (C-H). A C=O peak, the representative bonding of a carboxyl group, coexisted with the N-H peak at $1,500\text{--}1,700\text{ cm}^{-1}$ [23, 24]. These distinctive peaks of NTA were also observed in the FT-IR spectra of the NTA-attached particles on the PEI. These peaks were in contrast to the spectrum of PEI-attached Fe_3O_4 nanoparticles. Normally, most of differences on FTIR spectra of each NTA attached

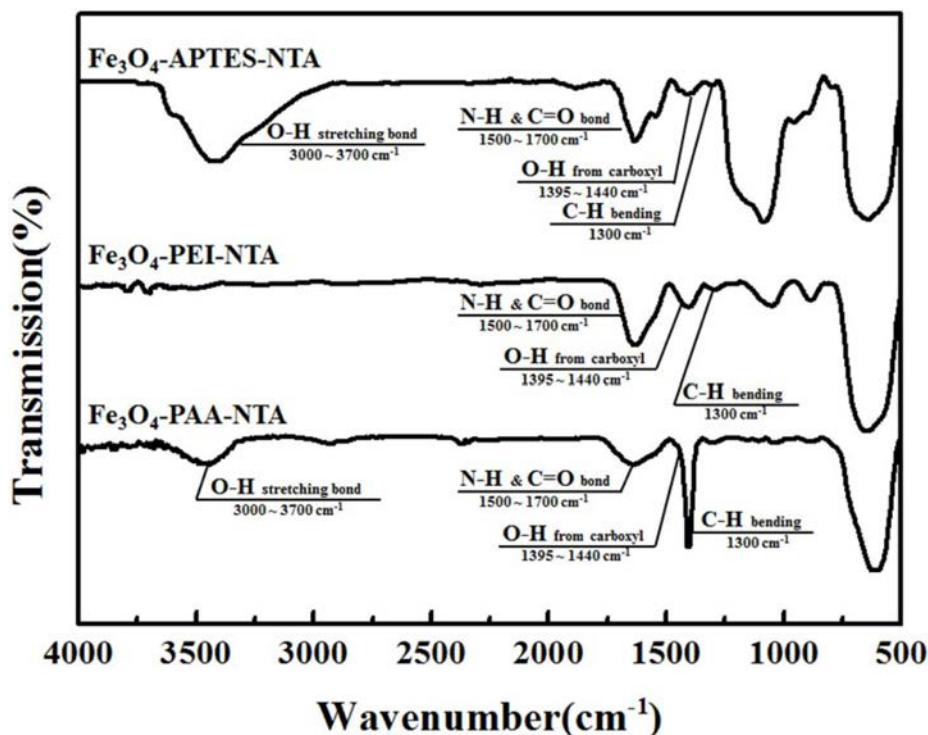


Fig. 4. FT-IR images of NTA conjugated Fe_3O_4 particles through various types of intermediate functionalization.

particle could be found almost same with that of amino-functionalized specimen [14, 22, 23]. In contrast, NTA-attached Fe_3O_4 nanoparticles obtained via carboxylic functionalization with PAA had distinctive NTA peaks at $1,300\text{ cm}^{-1}$ (C-H), $1,395\text{--}1,440\text{ cm}^{-1}$ (O-H), and $1,500\text{--}1,700\text{ cm}^{-1}$ (N-H and C=O co-exist), similar to other APTES- and PEI-treated particles; however, their intensities were lower than those of other samples [22]. Additionally, the O-H stretching bond was shifted to $3,000\text{--}3,700\text{ cm}^{-1}$, which was $2,700\text{--}3,300\text{ cm}^{-1}$ from the PAA-treated particles. Considering these differences between the amino- or carboxylic-functionalized and NTA-conjugated particles, it could be suggested that NTA was successfully attached to the surface of the Fe_3O_4 particles.

Functional group on the NTA conjugated Fe_3O_4

In the TEM image of NTA attached on the APTES used Fe_3O_4 particle from Fig. 5, core-shell structure was observed spherical shaped Fe_3O_4 core and fluffy shell. The size of the core material was approximately 300 nm, and the surface of the coated layer was observed to be wavy. However, the particles were covered with a coated layer under the agglomerated state, instead of being individually coated. The thickness of the coated layer was measured to be $15\text{--}30\text{ nm}$, which was greater than that of APTES-treated particle. In contrast, in the image of the PEI-treated Fe_3O_4 particles, round particles with a size of 300 nm were observed along with other small particles ($150\text{--}250\text{ nm}$ in size). These particles were agglomerated and linked with a

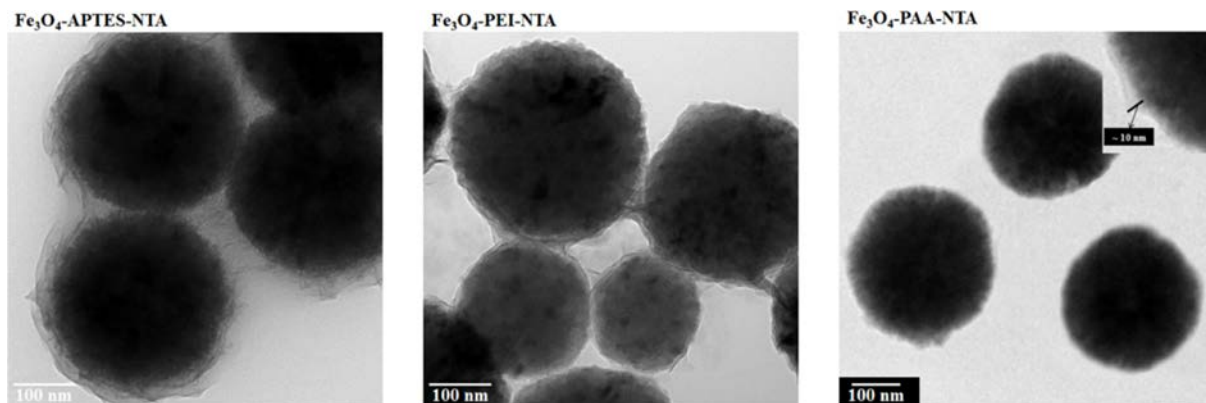


Fig. 5. TEM spectra of NTA conjugated Fe_3O_4 particles through various types of intermediate functionalization.

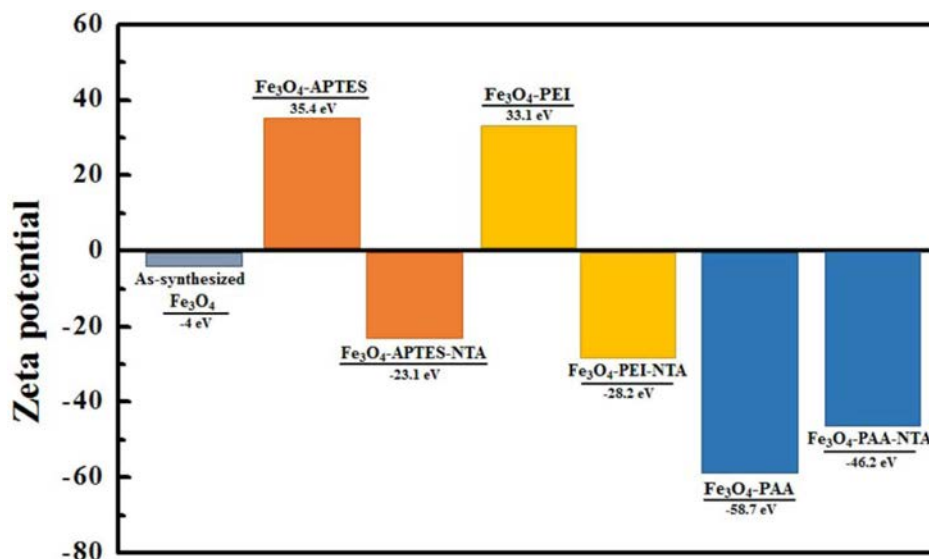


Fig. 6. Surface charge of as-synthesized, intermediate functionalized, and NTA conjugated Fe_3O_4 nanoparticles.

thin coated layer (8 ~ 15 nm). In the case of the PAA-treated particles, the sizes of the core Fe_3O_4 particles were observed to be around 300 nm, similar to APTES- and PEI-treated particles; however, unlike other samples, these PAA-treated particles remained separated. The coated layer covered the Fe_3O_4 nanoparticles individually and observed around 10 nm.

Differences about NTA conjugated Fe_3O_4 with various kind of intermediate functionalization

Thus, the NTA was successfully attached to the surface of the Fe_3O_4 nanoparticles, with the appearance of O–H and C–H peaks in the FT-IR spectrum of NTA-attached particles obtained via APTES or PEI treatment; hence, it was difficult to identify the C=O bonds owing to the existence of N–H peaks. However, these distinctive peaks were also observed in the FT-IR spectrum of the NTA-attached particles with PAA. Because NTA was conjugated with the same peptide bonding, it could be assumed that the pH values of APTES-, PEI-, and PAA-treated particles or the existence of a cross-linker affected the formation of the peptide bond. Hence, owing to these differences in the FT-IR spectra, the thickness of the coated layer of each NTA-attached particle increased; thus, NTA was observed to be successfully conjugated on the surface of PAA-treated Fe_3O_4 . However, their coated status varied for different intermediate functional groups. In the case of the amino-functionalized particles with APTES or PEI, agglomeration occurred. However, for carboxylic functionalization with PAA, the particles remained separated. Additionally, because difference of pH values and used cross linker could be the cause of this result.

Surface charges of NTA conjugated Fe_3O_4 with various kind of intermediate functionalization

In order to analyze repulsion force on the particle

surface charge of each functionalization stage of Fe_3O_4 samples were exhibited at Fig. 6. As-synthesized Fe_3O_4 had a slight negative charge that could not produce a repulsive force sufficient for stable dispersion. However, after the APTES treatment, the surface charge increased to 35.4 eV owing to the positive amine group [26]. However, the NTA-conjugation positive charge was changed into a negative charge of -23.1 eV. A similar observation was made for the PEI-treated particles, the surface charge of which changed from 33.1 eV to -28.2 eV. However, after PAA treatment, a strong negative charge (-58.7 eV) was formed on the surface of the particle, which changed into -46.2 eV upon NTA attachment.

Magnetic properties of NTA conjugated Fe_3O_4 with various kind of intermediate functionalization

The hysteresis curves of as-synthesized Fe_3O_4 and NTA-attached samples obtained via APTES, PEI, and

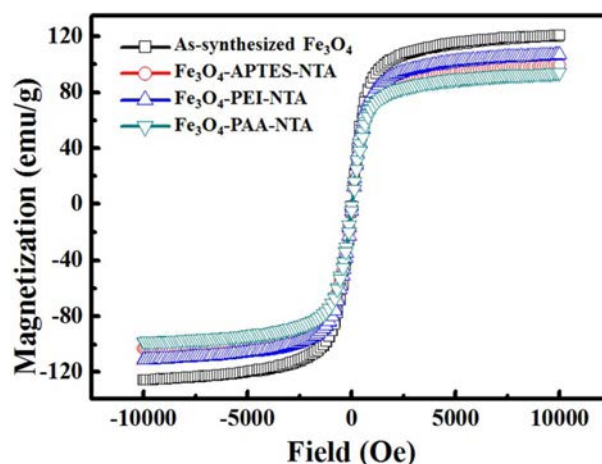


Fig. 7. Hysteresis loop of as-synthesized and NTA conjugated Fe_3O_4 nanoparticles.

PAA treatment are shown in Fig. 7. No coercivity or remnant magnetization was found in any of the hysteresis curves, and each particle exhibited paramagnetic curves. However, the saturated magnetization of as-synthesized Fe_3O_4 was the highest, with a value of 120 emu/g. This was followed by the APTES- and PEI-treated samples, which exhibited values of 106 and 98 emu/g, respectively; these values were 88.3% and 81.7% of largest value of saturated magnetization, respectively. The PAA-treated particles exhibited the lowest value, 94 emu/g, which was 78.3% of that of as-synthesized Fe_3O_4 .

Review about NTA conjugated Fe_3O_4 with various kind of intermediate functionalization

NTA was observed to be attached properly with the negative surface charge after the NTA-attaching process. However, the inversion of surface charge occurred in the amino-functionalized samples with APTES and PEI. During this inversion, owing to the pH inversion and changed functional group, the electrostatic force was weakened, and it was difficult to maintain their dispersion stability; thus, agglomeration occurred, which can be observed in the TEM images mentioned above. The PAA-treated particles, however, underwent a slight decline during the NTA conjugation process, and this charge was still strong enough for the dispersion. Meanwhile, the magnetization of the NTA-attached specimens was directly related to the reversible separation and re-dispersion, considering the high saturated magnetization and low remnant magnetization of these specimens. The magnetic hysteresis curves of each specimen originated from its Fe_3O_4 core particle and differed owing to the coated layer or phase variation resulting from external circumstances. During NTA conjugation via amino or carboxylic functionalization, the Fe_3O_4 nanoparticles underwent basic or acidic condition, which could damage the magnetic particles. However, their paramagnetic properties remained intact, and their saturated magnetization was sufficiently high for magnetic separation after the NTA attachment.

Conclusion

In this study, chelate-functionalized Fe_3O_4 nanoparticles were fabricated through intermediate functionalization with APTES, PEI, and PAA, and characterized for further applications, which can be derived using metal-ion chelating. The peaks of the FT-IR spectra indicated the alternation of the surface functional group according to the progression from the Fe_3O_4 nanoparticle synthesis to the NTA attachment. Specifically, after NTA attachment, distinctive peaks of NTA were observed, which were derived from the carboxyl group, amine group, and peptide bonding. After NTA attachment, the surface charge of the Fe_3O_4 nanoparticles was slightly weakened, and electronic inversion occurred through amino functionalization. Owing to the temporary lack of electrostatic

repulsive force due to the electronic inversion, the APTES- and PEI-treated particles were covered with an NTA layer under an agglomerated state, unlike the PAA-treated particles.

In conclusion, NTA was successfully attached to the surface of Fe_3O_4 nanoparticles through functionalization using APTES, PEI, and PAA. Owing to the various functionalization chemicals, the dispersion properties of the NTA-attached Fe_3O_4 particles were different. By further analyzing metal-ion chelating and separating biomaterials, such as his-tag or DNA, NTA-attached superparamagnetic nanoparticles can be used in various applications.

Acknowledgement

This work was supported by “Human Resources Program in Energy Technology” of the KETEP and MOTIE of the Republic of Korea (No. 20194030202450) and by the National Research Foundation of Korea (NRF) grant funded by the Korea government (MSIP) (2018R1A5A6075959).

References

1. M.T. Gabr and F.C. Pigge, Dalton T. 45 (2016) 14039-14043.
2. G.R. You, G.J. Park, S.A. Lee, K.Y. Ryu, and C. Kim, Sensor Actuat. B-Chem. 215 (2015) 188-195.
3. N.V. Petrochenkova, A.G. Mirochnik, T.B. Emelina, A.A. Sergeev, A.A. Leonov, and S.S. Voznesenskii, Spectrochim Acta A Mol. Biomol. Spectrosc. 200 (2018) 70-75.
4. F. Tudorache, I. Petrila, T. Slatineanu, A.M. Dumitrescu, A.R. Iordan, M. Dobromir, and M.N. Palamaru, J. Mater. Sci.: Mater. 27 (2015) 272-278.
5. S.-L. Kao, P. Venkatesan, and S.-P. Wu, New J. Chem. 39 (2015) 3551-3557.
6. N.E. Boland and A.T. Stone, Geochim. Cosmochim. Acta 212 (2017) 176-195.
7. W. Dong, Y. Bhide, S. Marsman, M. Holtrop, T. Meijerhof, J. de Vries-Idema, A. de Haan, and A. Huckriede, Biotechnol. J. 13 (2018) 1700645.
8. L. Li, Z. Huang, X. Fan, Z. Zhang, R. Dou, S. Wen, Y. Chen, Y. Chen, and Y. Hu, Electrochim. Acta 231 (2017) 354-362.
9. J. Li, L. Zhang, G. Wei, Y. Zhang, and Y. Zeng, Biosens. Bioelectron 69 (2015) 316-320.
10. A. Dutta Chowdhury, N. Agnihotri, R.A. Doong, and A. De, Anal Chem 89 (2017) 12244-12251.
11. Y. Xin, X. Fu-bing, L. Hong-wei, W. Feng, C. Di-zhao, and W. Zhao-yang, Electrochim. Acta 109 (2013) 750-755.
12. C. Zhang, S. Si, and Z. Yang, Biosens. Bioelectron 65 (2015) 115-120.
13. S. Hu, W. Ouyang, L. Guo, Z. Lin, X. Jiang, B. Qiu, and G. Chen, Biosens. Bioelectron 92 (2017) 718-723.
14. H. Guo, M. Li, S. Tu, and H. Sun, IOP Conf. Ser.: Mater. Sci. Eng. 322 (2018) 022017.
15. Y. Wang, J. Dostalek, and W. Knoll, Anal. Chem 83 (2011) 6202-6207.
16. Q. Wu, Y. Sun, D. Zhang, S. Li, X. Wang, and D. Song, Biosens. Bioelectron 86 (2016) 95-101.

17. S. Yao, X. Yan, Y. Zhao, B. Li, and L. Sun, *Mater. Lett.* 126 (2014) 97-100.
18. G. Harris, T. Palosaari, Z. Magdolenova, M. Mennecozzi, J.M. Gineste, L. Saavedra, A. Milcamps, A. Huk, A.R. Collins, M. Dusinska, and M. Whelan, *Nanotoxicology* 9 (2015) 87-94.
19. G.S. An, S.W. Choi, D.H. Chae, H.S. Lee, H.-J. Kim, Y. Kim, Y.-G. Jung, and S.-C. Choi, *Ceram. Int.* 43 (2017) 12888-12892.
20. G.S. An, J.S. Han, J.R. Shin, D.H. Chae, J.U. Hur, H.-Y. Park, Y.-G. Jung, and S.-C. Choi, *Ceram. Int.* 44 (2018) 12233-12237.
21. S. Li, K. Yang, L. Liu, B. Zhao, Y. Chen, X. Li, L. Zhang, and Y. Zhang, *Anal. Chim. Acta* 997 (2018) 9-15.
22. G.S. An, S.W. Choi, T.G. Kim, J.R. Shin, Y.-I. Kim, S.-C. Choi, and Y.-G. Jung, *Ceram. Int.* 43 (2017) 157-161.
23. G.S. An, J.R. Shin, J.U. Hur, A.H. Oh, B.-G. Kim, Y.-G. Jung, and S.-C. Choi, *J. Alloy. Compd.* 798 (2019) 360-366.
24. G.S. An, J.S. Han, J.R. Shin, J.H. Cha, B.-G. Kim, Y.-G. Jung, and S.-C. Choi, *J. Alloy. Compd.* 792 (2019) 1008-1012.
25. J.S. Han, G.S. An, B.G. Park, and S.-C. Choi, *J. Korean. Ceram. Soc.* 55 (2018) 80-84.
26. J.U. Hur, J.S. Choi, S.-C. Choi, and G.S. An, *J. Korean. Ceram. Soc.* 57 (2020) 80-84.
27. A.H. Oh, H.-Y. Park, Y.-G. Jung, S.-C. Choi, and G.S. An, *Ceram. Int.* 46 (2020) 10723-10728.